Electronic Supplementary Material (ESI) for RSC Advances.

Electronic Supplementary Information

Surface and interface interplay on the oxidizing temperature of iron oxide and Au-Iron oxide core-shell nanoparticles

Sarveena[a], Diego Muraca[b,h], Pedro Mendoza Zélis[c], Y. Javed[d], N. Ahmad[e], J. M. Vargas[f], O. Moscoso-Londoño[b], M. Knobel[b,i], M. Singh[a]and S. K. Sharma[g,a*]

[a]Department of Physics, H. P. University, Shimla, 171005, HP India

[b]instituto de Física Gleb Wataghin, Universidade Estadual de Campinas (UNICAMP) 13083-859 SP, Brazil

[c]Instituto de Física de La Plata (IFLP- CONICET), Departamento de Física, Facultad de Ciencias Exactas, Universidad Nacional de La Plata (UNLP), c.c. 67, 1900 La Plata, Argentina

[d]Department of Physics, University of Agriculture, Faisalabad, Pakistan

[e]Laboratoire Matériaux et Phénomènes Quantiques, UMR 7162 CNRS/Université Paris Diderot, 10 rue Alice Domon et Léonie Duquet, Paris F-75205 Cedex 13, France,

[f]Centro Atomico Bariloche (CNEA), Instituto Balseiro (U. N. Cuyo) and Conicet, 8400 San Carlos de Bariloche, Río Negro, Argentina

[g]Departamento de Física, Universidade Federal do Maranhão, 65085-580 São Luis, Brazil

[h]Centro de Ciencias Naturais e Humanas, Universidade Federal do ABC-UFABC, Av. dos Estados, 5001, Santo André, Brazil

[i]Laboratorio Nacional de Nanotecnologia (LNNano/CNPEM), Rua Giuseppe Máximo Scolfaro 10000, 13083-100, Campinas-SP, Brazil

*surender76@gmail.com

(a) X-ray diffraction for the fresh and one year old sample of iron oxide nanoparticles:

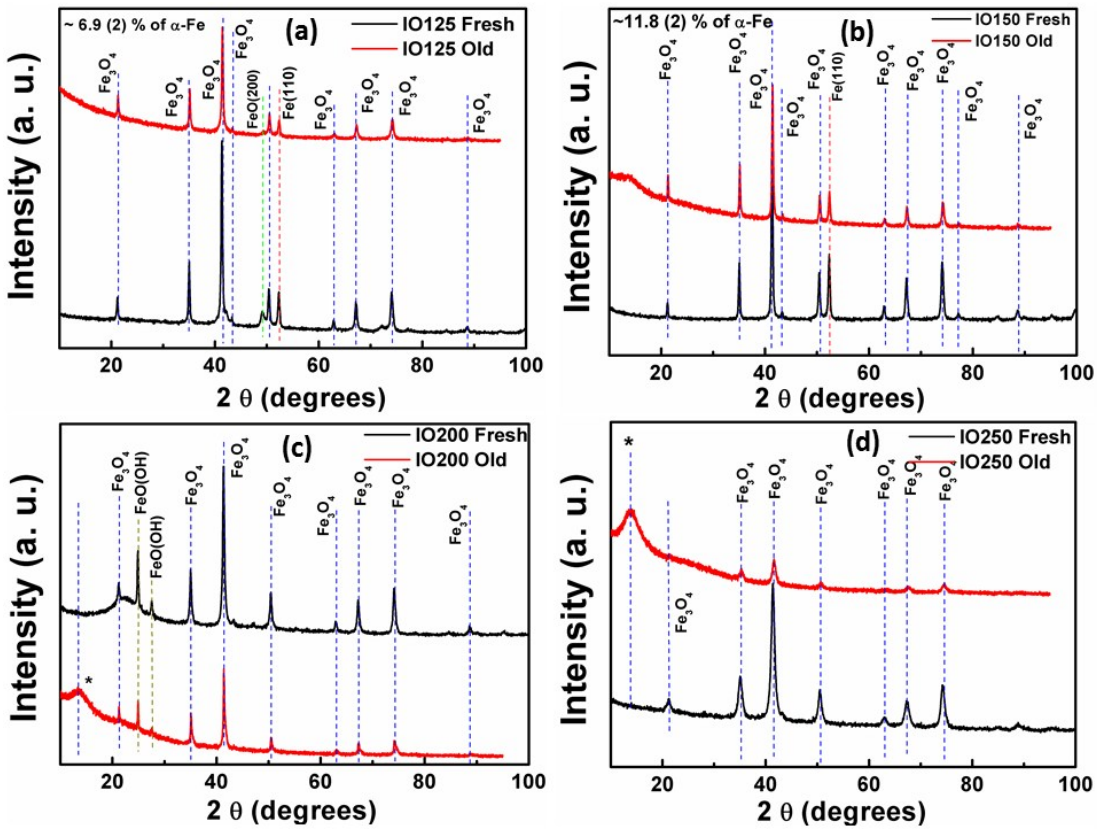

Figure S1 X-ray diffraction of the fresh and one year old sample of iron oxide nanoparticles, (a) IO 125, (b) IO150, (c) IO200, and IO250.

(b) Small angle x-ray scattering curves for the fresh iron oxide nanoparticles:

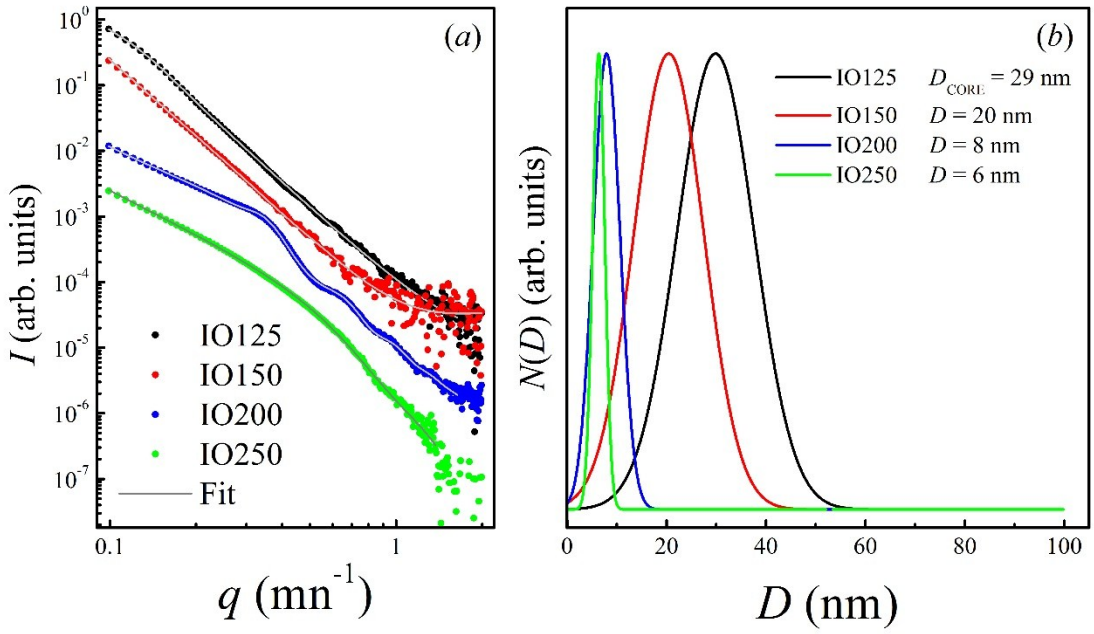

Figure S2. (*a*) Double-logarithmic representation of colloid scattering curves. (b) fitted Gaussian size distribution for iron oxide nanoparticles.

The figure S2 (a) shows the double logarithmic representation of small angle x-ray scattering curves for samples IO125, IO150, IO200 and IO250. Due to the diversity in the nanoparticle size, dispersity and possible cluster effects, one can see differences among the scattering profiles. i.e., at low *q* region all scattering patterns reveals different, but a well-marked power law behaviors instead of the typical Guinier behavior of a single particle systems, which is a distinctive signature of systems composed by polydisperse and agglomerate particles. At the intermediate *q* region (0.5 – 1 nm^{-1}), the scattering profile of sample IO200 presents a finger form, which is typical of nanoparticle systems with finite-size distribution [1]. Such feature is not observed for the others IO samples, thereby indicating that the polydispersity and the effects associated to the scattering interference between the neighboring particles are more

relevant in samples IO125, IO150 and IO250. For q values larger than 1.5 nm^{-1}, the scattering profile behavior is masked by an incoherent background [2].

In order to take into account the single or core-shell (revealed by TEM for IO125) nanoparticle aggregation, each SAXS experimental pattern was fitted assuming that the scattered intensity I (q) is composed by one or two different scattering contributions (depending on the sample). In this sense, the intensity I(q) from a collection of particles can be described by:

$$I(q) = I_1(q) + I_2(q) + bkg,$$

where I_1 (q) and I_2 (q) are the scattering contributions, which each one can be rewritten as the product of a form factor (P(q)) and a structure factor (S(q)). An invariant q term was added in order to consider the incoherent background (bkg). Because of the complexity and differences of the multiphase systems under study, we have chosen deferments form factors and structure factors to fit the experimental SAXS data (see Table 1).

Table 1 contains the form and structure factors used to fit each SAXS data

Sample	$I_1(q)$		$I_2(q)$	
	$P_1(q)$	$S_1(q)$	$P_2(q)$	$S_2(q)$
IO125	$\int_0^\infty [K(q,r+\Delta R,\Delta\eta_1) - K(q,r,\Delta\eta_2 - \Delta\eta_1)]^2 f(r)dr$ Core-shell form factor	$1+\frac{D_F\Gamma(D_F-1)\sin[(D_F-1)\tan^{-1}(q\xi)]}{(qr)^{D_F}[1+1/(q\xi)^2]^{(D_F-1)/2}}$ Mass fractal structure factor	$\int_0^\infty K^2(q,r,\Delta\eta)f(r)dr$ polydisperse spherical particles	$\frac{1}{1+24f_p\frac{G(f_p,qr)}{qr}}$ hard sphere structure factor
IO150			-----	-----
IO200	$\int_0^\infty K^2(q,r,\Delta\eta)f(r)dr$ Polydisperse spherical particles		$\int_0^\infty K^2(q,r,\Delta\eta)f(r)dr$ polydisperse spherical particles	$\frac{1}{1+24f_p\frac{G(f_p,qr)}{qr}}$ hard sphere structure factor
IO250			-----	-----

For samples *IO150*, *IO200* and *IO250,* the scattering of diluted polydisperse spherical particles is given by $K=\frac{4}{3}\pi r^3\Delta\eta 3\frac{\sin(qr)-qrcos(qr)}{(qr)^3}$, being $\Delta\eta$ is the scattering length density difference between nanoparticles and the solvent. For sample, *IO125* was chosen the core-shell form factor for polydisperse spherically symmetric particles with mean radius size *R* and shell thickness Δ*R* (according with TEM information), in which $\Delta\eta_1$ and $\Delta\eta_2$ are the scattering length density difference between the core or shell and the solvent, respectively. As can be noted, for the first scattering contribution (I_1 (q)) was chosen the same structure factor (S_1 (q)), which was postulated by Chen and Teixeira in the framework of the fractal aggregate model. Here,

$\Gamma(D_F - 1)$ is the gamma function and D_F is the fractal dimension. The parameter ξ is the finite cluster size that appears in the $h(r_0,\xi)$ cut-off function. Such function describes the perimeter of the aggregate (in our case, $h(r_0,\xi) = \exp\left[-r_0/\xi\right]$). For samples IO150 and IO250 a well fit was achieved by using only one scattering contribution ($I_1(q)$) with the form and structure factors already mentioned, while for samples IO125 and IO200 was necessary to use one more scattering contribution ($I_2(q)$). In these two samples, we use the same form factor (polydisperse spherical particles) than in first scattering contribution, but this time we used a hard sphere structure factor ($S_2(q)$) to consider the interparticle interference effects [3]. In this, f_P is the local volume fraction of the spherical particles within the clusters, which is related to the probability of finding particles in the vicinity of each other. In all cases, it was considered a Gaussian radii distribution $f(r) = \frac{1}{\sigma\sqrt{2\pi}} e^{-(r-R)^2/2\sigma^2}$, being R the mean particle radius and σ the standard deviation. Obtained fitting parameters are summarized in Table 2.

Table 2 SAXS fitted parameters. D, ΔR, ξ, D_F, and f_P (defined in the text) obtained from the curve fitting according to form and structure factors registered on Table 1.

Sample	D (nm)	ΔR	ξ (nm)	D_F	f_P
IO125	29	1.3	53	2.93	0.27
IO150	20	----	108	2.90	----
IO200	8	----	20	1.30	0.44
IO250	6	----	20	1.92	----

The primary particle size distribution is shown in Figure S2(b) and the corresponding values are reported in table 2. It is observed that the average particle diameters are 29 nm (core), 20 nm 8.0 nm and 6.0 nm for samples IO125, IO150, IO200 and IO250, respectively. These values are consistent with the nanoparticles diameters calculated by TEM and XRD. The layer thickness of

the sample IO125 also matches well with the information obtained by TEM. On the other hand, values of the cluster size (ξ) and the fractal dimension (D_F) for samples IO125 and IO150 are representative of system with larger and compact aggregates.

(c) TEM images and Particle Size distribution:

Iron Oxide nanoparticles:

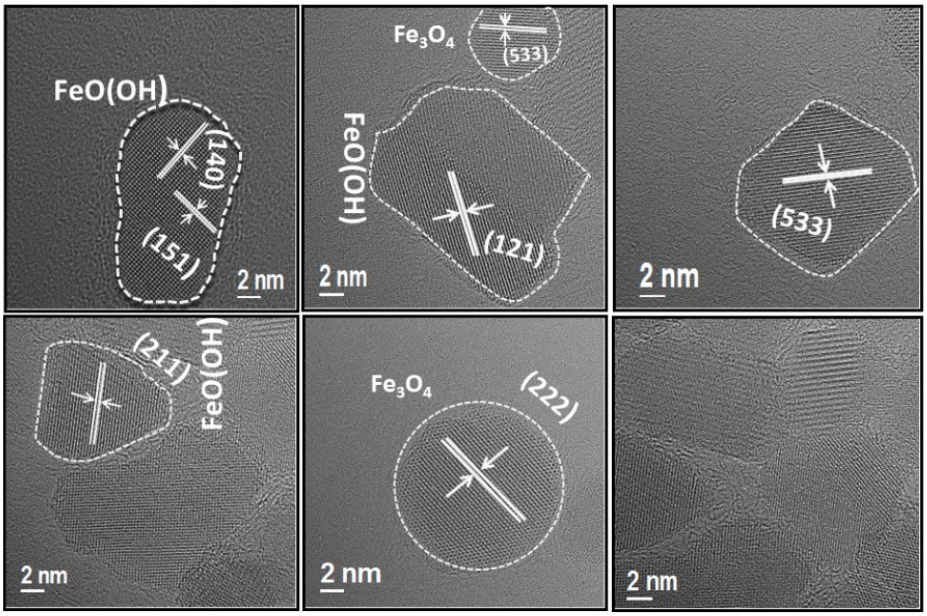

Figure S3 (a-f) HRTEM images of iron-oxide nanoparticles (IONPs) oxidized at 200^{o}C for 30 minutes during cooling from 315^{o}C.

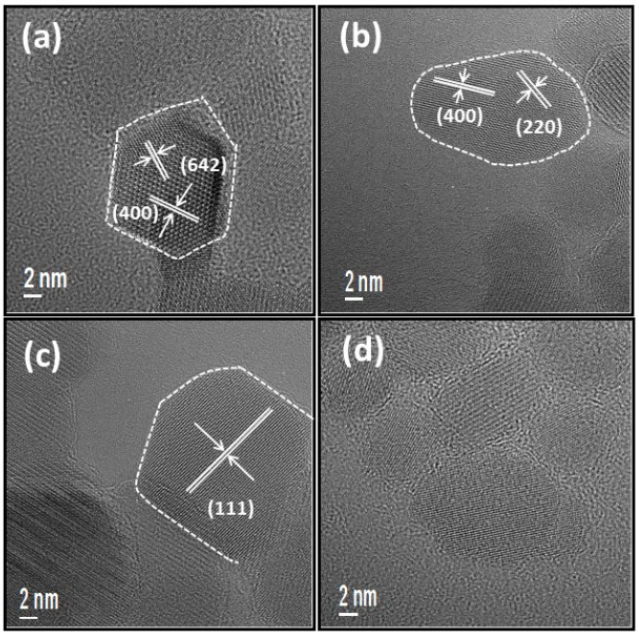

Figure S4 (a-d) HRTEM images of the iron oxide nanoparticles (IONPs) oxidized at 250^{o}C for 30 minutes during cooling from 315^{o}C.

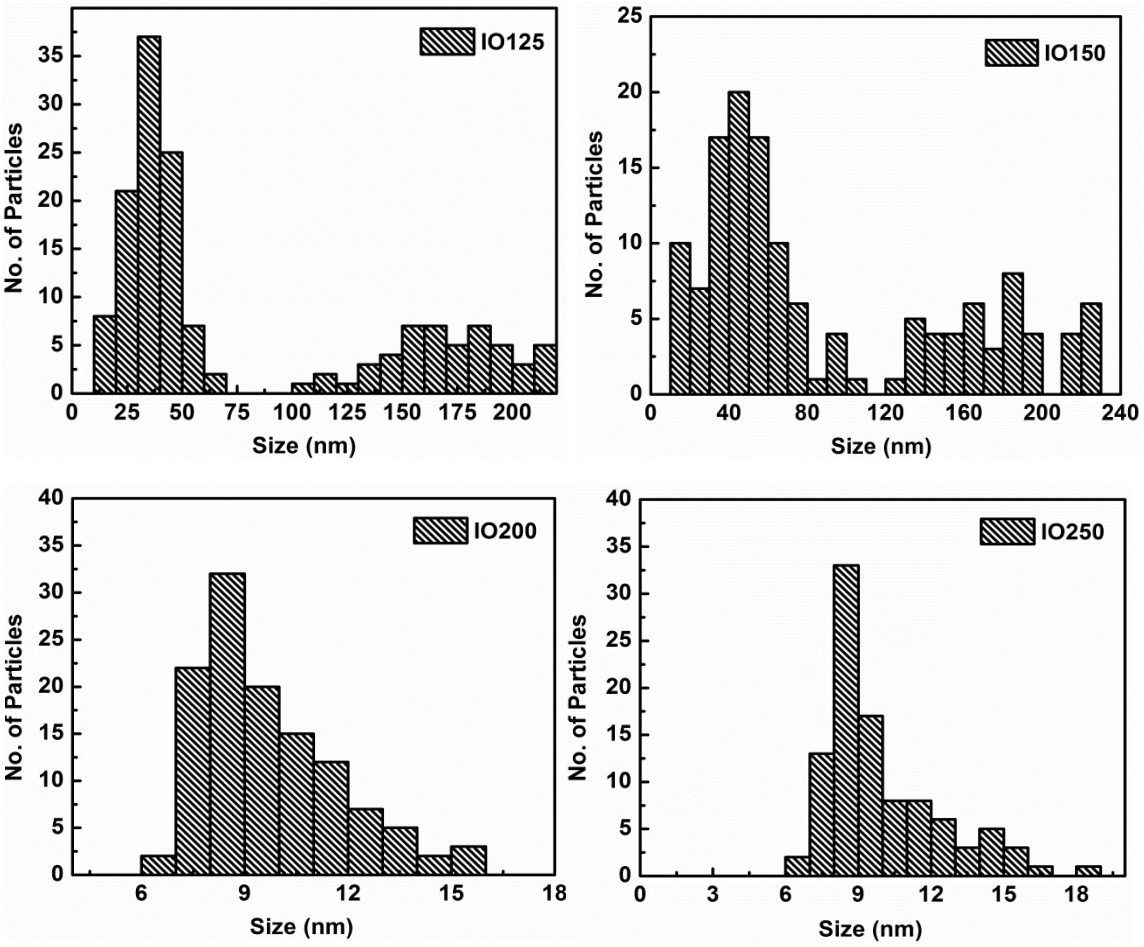

Figure S5 Particle size histograms derived by counting at least 100 particles for the Iron oxide nanoparticles.

Au Nano seeds:

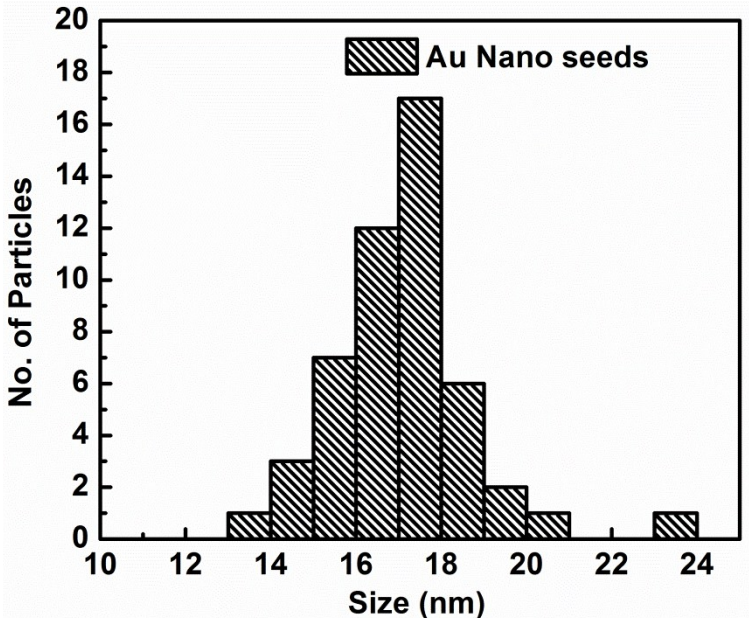

Figure S6 Particle size histograms for the Au nanoparticles.

AIO Nanoparticles:

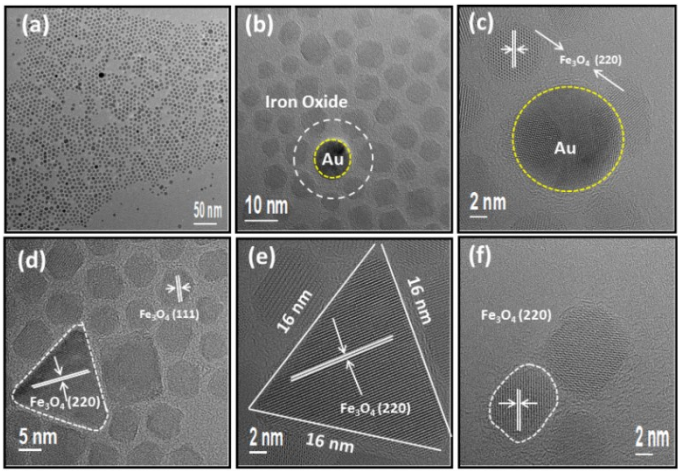

Figure S7 (a-f) HRTEM images of Au-iron oxide nanoparticles oxidized at 125°C for 30 minutes during cooling from 315°C.

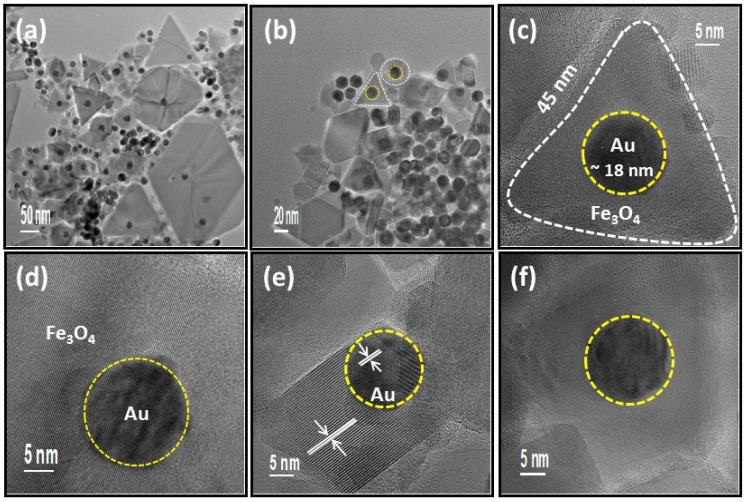

Figure S8 (a-f) HRTEM images of iron oxide nanoparticles oxidized at 150°C for 30 minutes during cooling from 315°C

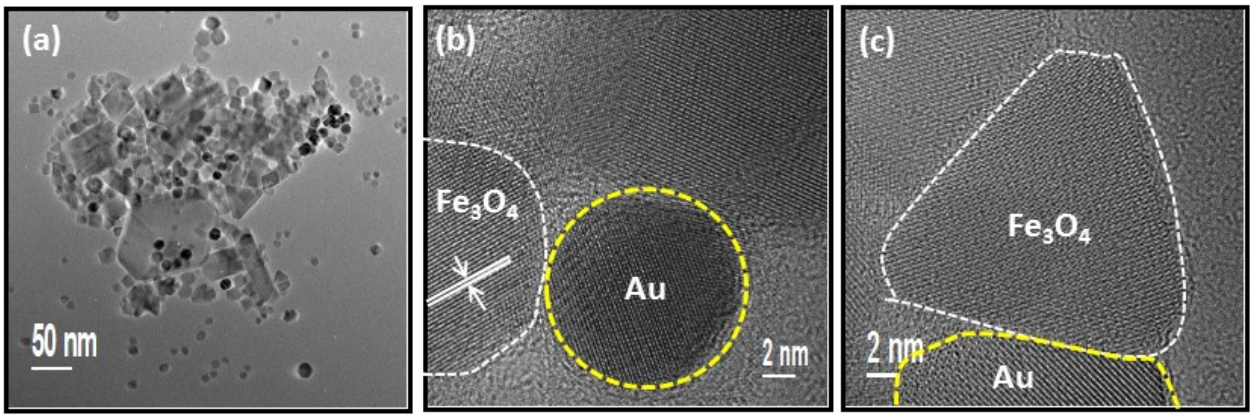

Figure S9 (a-c) HRTEM images of iron oxide nanoparticles oxidized at 200^{o}C for 30 minutes during cooling from 315^{o}C

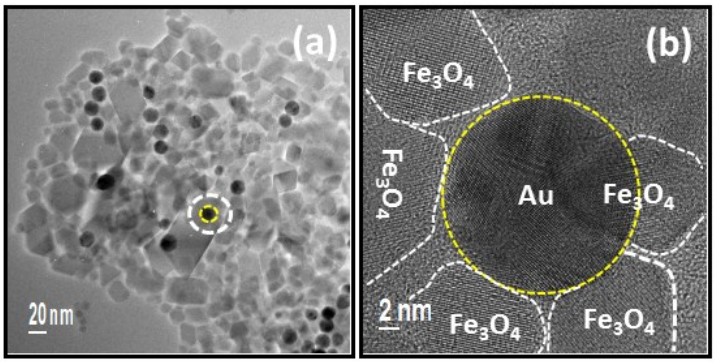

Figure S10 HRTEM images for iron oxide nanoparticles oxidized at 250^{o}C for 30 minutes during cooling from 315^{o}C.

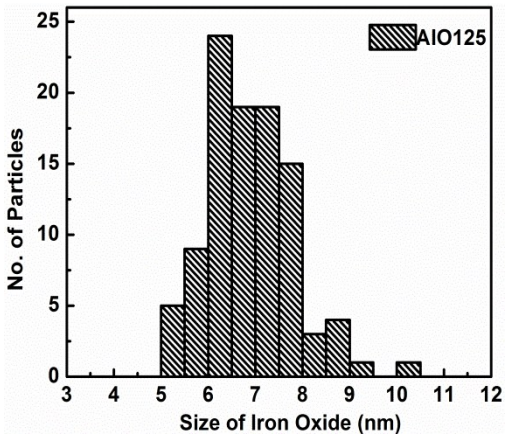

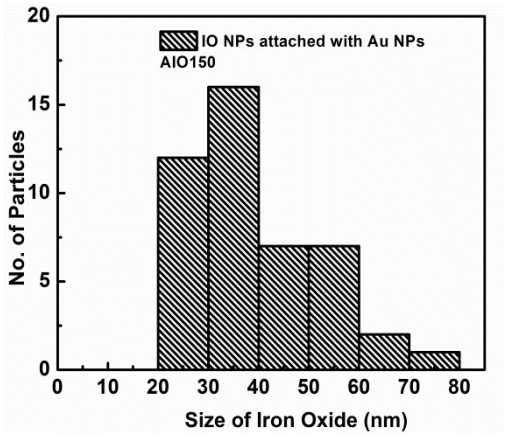

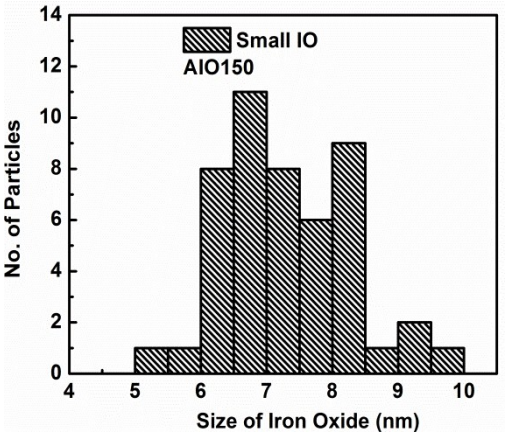

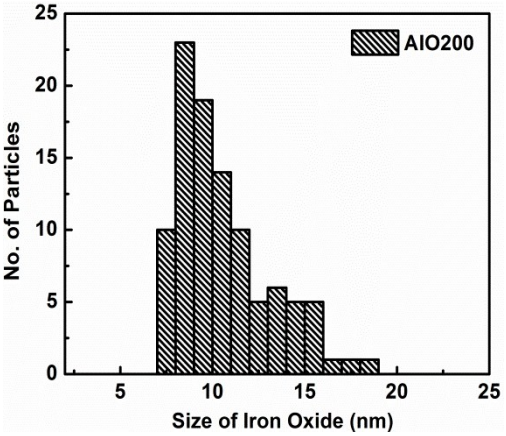

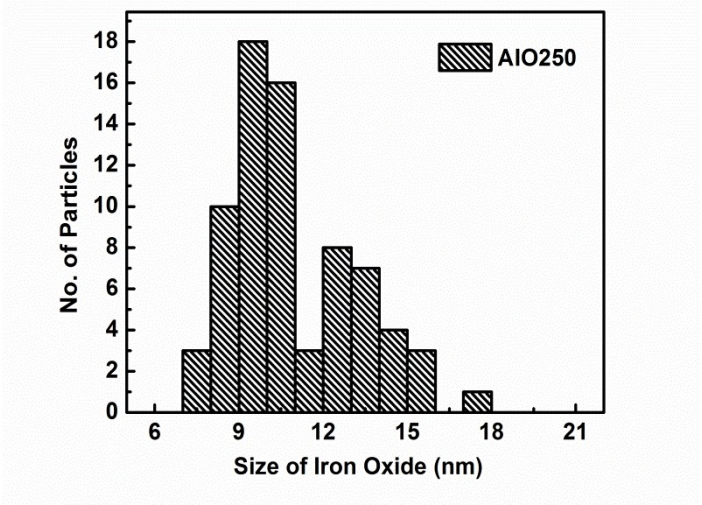

Figure S11 Particle size histograms derived by counting at least 100 particles for the Iron oxide nanoparticles.

TABLE III Nanocomposites sizes calculated from the Scherrer equation (XRD) and TEM imaging, (a) iron oxide, and (b) Au-iron oxide

(a)

Sample	XRD Scherrer's formula (nm)	TEM Mean (nm)/Std. dev.
IO125	35.6	39 ± 3.0
IO150	36.7	38 ± 2.5
IO200	26.6	12 ± 2.0
IO250	12.6	10 ± 2.0

(b)

Sample	XRD Scherrer formula (nm)	TEM Mean (nm)/Std. dev.
AIO125	8.5	9.4 ± 3.0
AIO150	27.3	30 ± 2.5
AIO200	30.6	32 ± 2.3
AIO250	15.4	16 ± 2.0
Au NPs	13.4	14 ± 1.0

Table IV Lattice Parameters (in Å) for Samples IO125-IO250

Sample	(311)	(111)	(220)	(311)	(422)	(511)	(440)
IO125	8.369 Fe(110) 2.855 FeO(200) 4.181	4.845	2.960	2.522	1.706	1.608	1.477
IO150	8.364 Fe(110) 2.854	4.835	2.957	2.521	1.706	1.608	1.477
IO200	8.361 FeO(OH)(110) 5.838	4.832	2.956	2.520	1.705	1.607	1.476
IO250	8.352	4.844	2.953	2.518	1.704	1.605	1.474

Table V (a) Mossbauer hyperfine parameters iron oxide nanoparticles

Sample	Subspectrum	I.S (mm/s)	Q.S (mm/s)	H(T)	Area
IO125	1	0.98±0.02	0.59±0	-	3.85%
	2	0.28±0.003	-0.02	49.20±0.03	33.33%
	3	0.67±0.003	-0.02±0.005	46.02±0.02	40.79%
	4	0.006±0.005	0	33.24±0.04	13.99%
	5	0.38±0.02	0	43.09±0.4	7.71%
IO150	1	0.38±0.02	0.73±0.04	-	2.31%
	2	0.28±0.002	-0.02±0.004	49.39±0.02	36.07%
	3	0.67±0.002	0.0002±.004	46.22±0.02	41.0%
	4	-0.005±0.003	0	33.24±0.02	20.62%
IO200	1	0.29±0.005	-0.004±0.008	49.35±0.04	41.81%
	2	0.67±0.004	-0.003±0.007	46.25±0.04	45.48%
	3	0.63±0	0	42.28±0.9	12.71%
IO250	1	0.35±0.003	-0.01±0.005	48.89±0.05	46.15%
	2	1.11±0	0	40.88±0.6	27.69%
	3	0.37±0.01	-0.06±0.02	45.56±0.4	16.93%

	4	0	0	16.49±0.2	9.22%

Table V (b) Mossbauer hyperfine parameters of Au-iron oxide nanoparticles

Sample	Subspectrum	I.S (mm/s)	Q.S (mm/s)	H(T)	Area
AIO125	1	0.35±0.01	-	-	42.66%
	2	0.334±0.008	0.67±0.012	-	6.05%
	3	0.34±0.05	0	-0.048±10797.001	49.03%
	4	0.34±0.07	0	47.842±0	2.26%
AIO150	1	0.278±0.05	-	-	26.29%
	2	0.31±0.004	-0.03±0.008	49.425±0.03	47.02%
	3	0.64±0.01	0.05±0.017	45.65±0.08	26.68%
AIO200	1	0.65±0.01	0.04±0.02	45.84±0.08	44.37%
	2	0.31±0.007	0±0.08	49.19±0	55.62%
AIO250	1	0.29±0.004	-0.02±0.005	48.69±0.02	32.20%
	2	0	0	43.86±0.6	13.42%
	3	0.63±0.007	-0.006 ±0	45.68±0.07	20.99%
	4	0	0	39.57±1.67	7.31%
	5	0.29±0.08	0	27.48±1.97	25.33%

Sample	TEM	Magnetite	Fe(II)	Fe(III)	α-Fe	Collective excitation	A (Fe^{3+})	B (Fe^{3+}/Fe^{2+})
IO125	39 ± 3.0	82%	4%	-	14%	7%	0.45	0.55
IO150	38 ± 2.5	77%	-	2%	21%	-	0.47	0.53
IO200	29 ± 2.0	100%	-	-	-	13%	0.48	0.52
IO250	15 ± 2.0	100%	-	-	-	53%	0.52	0.48
AIO125	9.4 ± 3.0	94%	-	6%	-	50% 42% SPM	-	-
AIO150	30 ± 2.5	100%	-	-	-	26%	0.66	0.33
AIO200	32 ± 2.3	100%	-	-	-	-	0.55	0.45
AIO250	16 ± 2.0	100%	-	-	-	47%	0.62	0.38

Table V (c) Mössbauer hyperfine parameters iron oxide and Au-iron oxide nanoparticles

References:

1. M. B. F. van Raap, P. M. Zélis, D. F. Coral, T. E. Torres, C. Marquina, G. F. Goya, and F. H. Sánchez. Self-organization in oleic acid-coated CoFe2O4 colloids: a SAXS study. J Nanoparticle Res 14, 2012, 1072.

2. C. Meiorin, O. Moscoso Londoño, D. Muraca, L. M. Socolovsky, K. R. Pirota, M. I. Aranguren, M. Knobel, and M. A. Mosiewickic, Magnetism and structure of nanocomposites made from magnetite and vegetable oil based polymeric matrices. Materials Chemistry and Physics, 175, 2016, 81.

3. J. K. Precus, and G. J. Yevick. Analysis of Classical Statistical Mechanics by Means of Collective Coordinates Phys. Rev. 10, 1958, 1.